Section S1. GEOS-Chem configuration and emission inventories

Table S1. GEOS-Chem model configuration

Science Options	Configurations
Version	Version 10-01 public release (06/17/2015)
Vertical Grid Mesh	72 Layers
Horizontal Grids	2x2.5 degree latitude/longitude
Initial Conditions	1 year full spin-up
Meteorology	Year-specific GEOS5 meteorology
Chemistry	
Chemistry mechanism	Benchmark mechanism which consists of the standard NOx-Ox-hydrocarbon-aerosol-bromine tropospheric chemistry mechanism (tropchem) plus the universal tropospheric-stratospheric chemistry extension (UCX) and secondary organic aerosols (SOA) species
Photolysis mechanism	FAST-JX (Eastham et al., 2014)
Horizontal Transport	
Advection Scheme	TPCORE
Vertical Transport	
Cloud convection scheme	Relaxed Arakawa-Schubert scheme (Moorthi and Suarez, 1992)
Stratosphere-troposphere exchange	UCX
Planetary Boundary Layer (PBL) mixing	Full PBL mixing (TURBDAY)
Dry deposition scheme	Resistance-in-series model (Wesely, 1989; Wang et al., 1998) for gaseous species and aerodynamic resistance scheme (Zhang et al., 2001) for aerosol species
Numerics	
Chemistry Solver	Kinetic Pre-Processor (KPP) solver using the Rosenbrock method
Parallelization	OpenMP

References:

Eastham, S. D., Weisenstein, D. K., Barrett, S. R. H., 2014, Development and evaluation of the unified tropospheric–stratospheric chemistry extension (UCX) for the global chemistry–transport model GEOS-Chem, Atmos. Environ., 89, 52–63.

Moorthi, S., Suarez, M. J., 1992, Relaxed Arakawa–Schubert: A parameterization of moist convection for general circulation models, Mon. Weather Rev., 120, 978–1002.

Wang, Y., Jacob, D.J., Logan, J.A., 1998, Global simulation of tropospheric O_3-NO_x-hydrocarbon chemistry, 1. Model formulation, J. Geophys. Res., 103(D9), 10,713–10,726.

Wesely, M. L., 1989, Parameterization of surface resistance to gaseous dry deposition in regional-scale numerical models, Atmos. Environ., 23, 1293–1304.

Zhang, L. M., Gong, S. L., Padro, J., Barrie, L., 2001, A size-segregated particle dry deposition scheme for an atmospheric aerosol module, Atmos. Environ., 35(3), 549–560.

Table S2. GEOS-Chem global anthropogenic emission inventories.

Source category	Inventory	Pollutants	Baseline year	Inventory Grid Definition	2010 Model Year
Biofuel ammonia	GEIA	NH_3	1998	GMAO 4x5	Used baseline inventory
All anthropogenic excluding shipping, aircraft and rails	EDGAR v4.2	CO, NO, SO_2, SO_4, NH_3	1970-2008	0.1x0.1	CO, NO, SO_2, SO_4 – projected to 2010 using GEOS-Chem default annual scaling factors NH_3 – 2008 inventory
Biofuel	Yevich and Logan, 2003	NO, CO, SO_2, VOCs (some VOC species are replaced with RETRO VOCs)	1985	GMAO 4x5	Used baseline inventory
Anthro VOCs	RETRO + Xiao et al, 2008 (C_2H_6)	VOCs	2000 (RETRO) 1985 (Xiao)	0.5x0.5 (RETRO) GMAO 1x1 (Xiao)	Used baseline inventory
Carbonaceous particles from fossil fuel and biofuel	Bond et al., 2007	BC, OC	2000	Generic 1x1	Used baseline inventory
Shipping	ARCTAS	SO2	2008	Generic 1x1	Projected to 2010 using GEOS-Chem default annual scaling factors
	ICOADS	CO, NO	2002	Generic 1x1	Projected to 2010 using GEOS-Chem default annual scaling factors
Aviation	AEIC	NO, CO, VOCs, SO_2, SO_4, BC, OC	2005	Generic 1x1	Used baseline inventory
Soil NOx by fertilizer	GEOS-Chem default	NO	2000	Generic 0.5x0.5	Used baseline inventory

References:

Bond, T.C., Bhardwaj, E., Rong, D., Jogani, R., Jung, S., Roden, C., Street, D.G., Trautmann, N.M., 2007, Historical emissions of black and organic carbon aerosol from energy-related combustion, 1850–2000, Global Biogeochem. Cycles, 21, GB2018.

Xiao, Y., Logan, J. A., Jacob, D. J., Hudman, R. C., Yantosca, R., Blake, D. R., 2008, Global budget of ethane and regional constraints on US sources, J. Geophys. Res., 113, D21306.

Yevich, R., Logan, J.A., 2003, An assesment of biofuel use and burning of agricultural waste in the developing world, Global Biogeochem. Cycles, 17(4), 1095.

Table S3. GEOS-Chem regional anthropogenic emission inventories[a]

Source category	Inventory	Pollutants	Baseline year	Inventory Grid Definition	2010 Model Year
US-only anthropogenic excluding biofuel	2011 NEI	NO, NO_2, HONO, CO, NH_3, VOCs, SO_2, SO_4, BC, OC	2006-2013	0.1x0.1	2010 inventory
Mexico	BRAVO	NO, CO, SO_2, SO_4	1999	Generic 1x1	projected to 2010 using GEOS-Chem default annual scaling factors
Canada	CAC	NO, CO, SO_2, SO_4, NH_3	2002-2008 2008 (NH_3)	GMAO 1x1	NO, CO, SO_2 – projected to 2010 using GEOS-Chem default annual scaling factors SO_4, NH_3 – 2008 inventory
Asia	MIX v1.1	NO, CO, SO_2, SO_4, NH_3, VOCs,	2008-2010	Generic 0.25x0.25	2010 inventory
Europe	EMEP	NO, CO, SO_2, SO_4, VOCs, NH_3	1990-2012 (NO, CO, SO_2, SO_4, NH_3) 1980-2000 (VOCs)	Generic 1x1 (NO, CO, SO_2, SO_4, NH_3) GMAO 1x1 (VOCs)	NO, CO, SO_2, SO_4, NH_3 – 2010 inventory VOCs – 2000 inventory

[a] GEOS-Chem, 2015. http://wiki.seas.harvard.edu/geos-chem/index.php/Anthropogenic_emissions#Regional_inventories, last access November 8, 2016.

Table S4. GEOS-Chem global natural emission inventories

Source category	Inventory	Pollutants	Baseline year	Inventory Grid Definition	2010 Model Year
Natural ammonia	GEIA	NH_3	1990	GMAO 4x5	Used baseline inventory
Biomass burning	GFED4	NO, CO, VOCs, SO_2, NH_3, BC, OC, POA1	1998-2014	Generic 0.25x0.25	2010 inventory
Biogenic	MEGAN v2.1	VOCs	1985	GMAO 1x1	Used baseline inventory
Seawater	GEOS-Chem default	DMS, ACET	1985 (DMS) 2005 (ACET)	GMAO 1x1 (DMS) Generic 1x1 (ACET)	Used baseline inventory
Short-lived bromo-carbon	Liang et al., 2010	$CHBr_3$, CH_2Br_2	2000	GMAO 2x2.5	Used baseline inventory
Volcanic	AEROCOM	SO_2	1979-2009	Generic 1x1	2009 inventory
Soil NO_x by nature	GEOS-Chem default	NO	2000	Generic 0.25x0.25	Used baseline inventory
Lightning NO_x	OTD-LIS	NO	1985	GMAO 2x2.5	2010 met files are used to adjust 1985 data
Dust	DEAD	Dust	1985	GMAO 4x5	Used baseline inventory
Background methane	GEOS-Chem default	CH_4	1983-2007		2007 data: Lat. 90N–30N, 1856 ppb Lat. 30N – 0, 1801 ppb Lat. 0–30S, 1742 ppb Lat 30S–90S, 1733 ppb

Reference:

Liang, Q., Stolarski, R. S., Kawa, S. R., Nielsen, J. E., Douglass, A. R., Rodriguez, J. M., Blake, D. R., Atlas, E. L., Ott, L. E., 2010. Finding the missing stratospheric Br_y: A global modeling study of CHBr3 and CH2Br2, Atmos. Chem. Phys., 10, 2269–2286.

Section S2. GEOS-Chem simulations

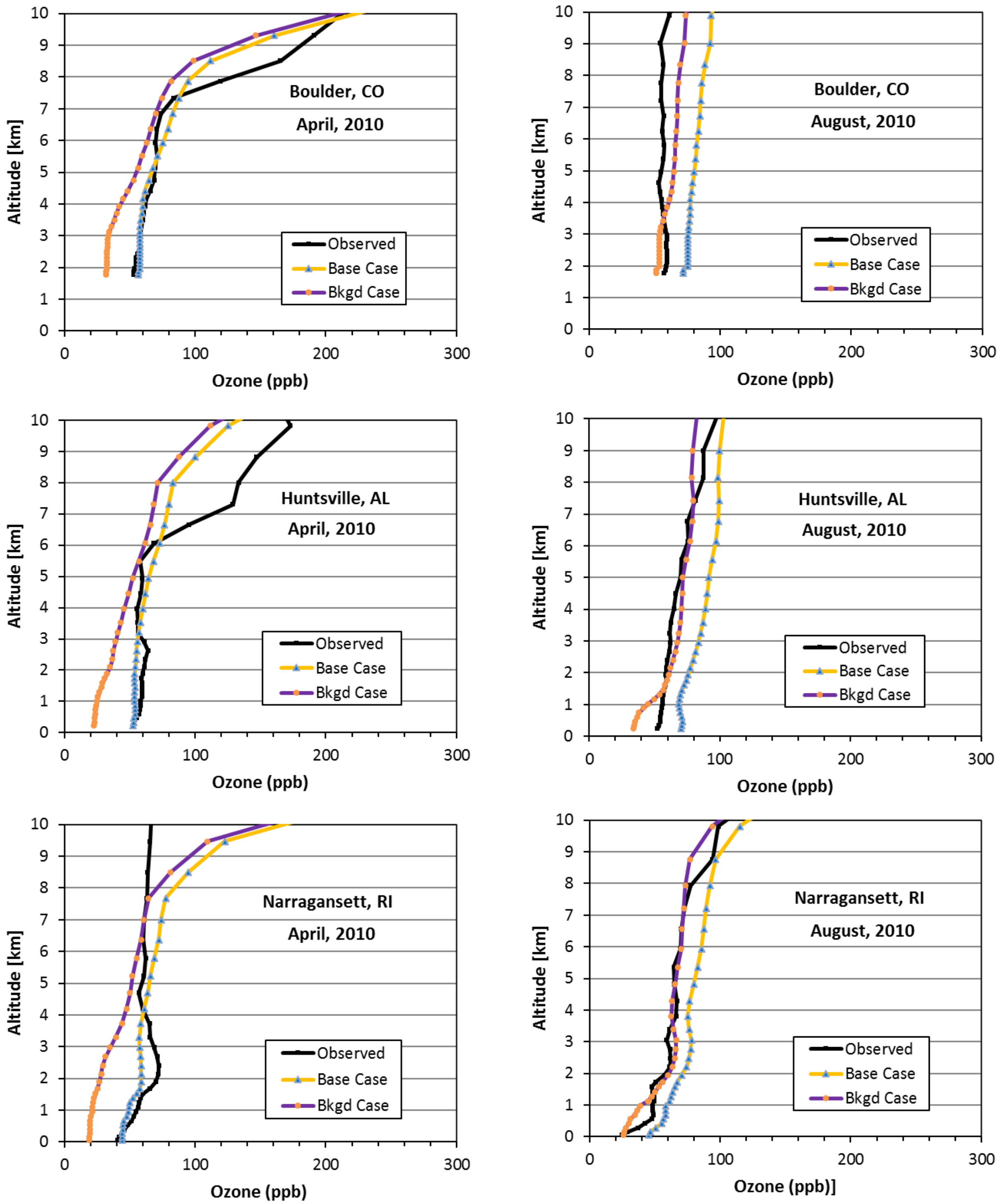

Figure S1. Comparison of GEOS-Chem vertical O_3 profiles for the base and background cases in April and August to ozonesonde measurements at three sites in the continental US. Monthly averages are shown. Locations and elevations of the sites are in Table S5.

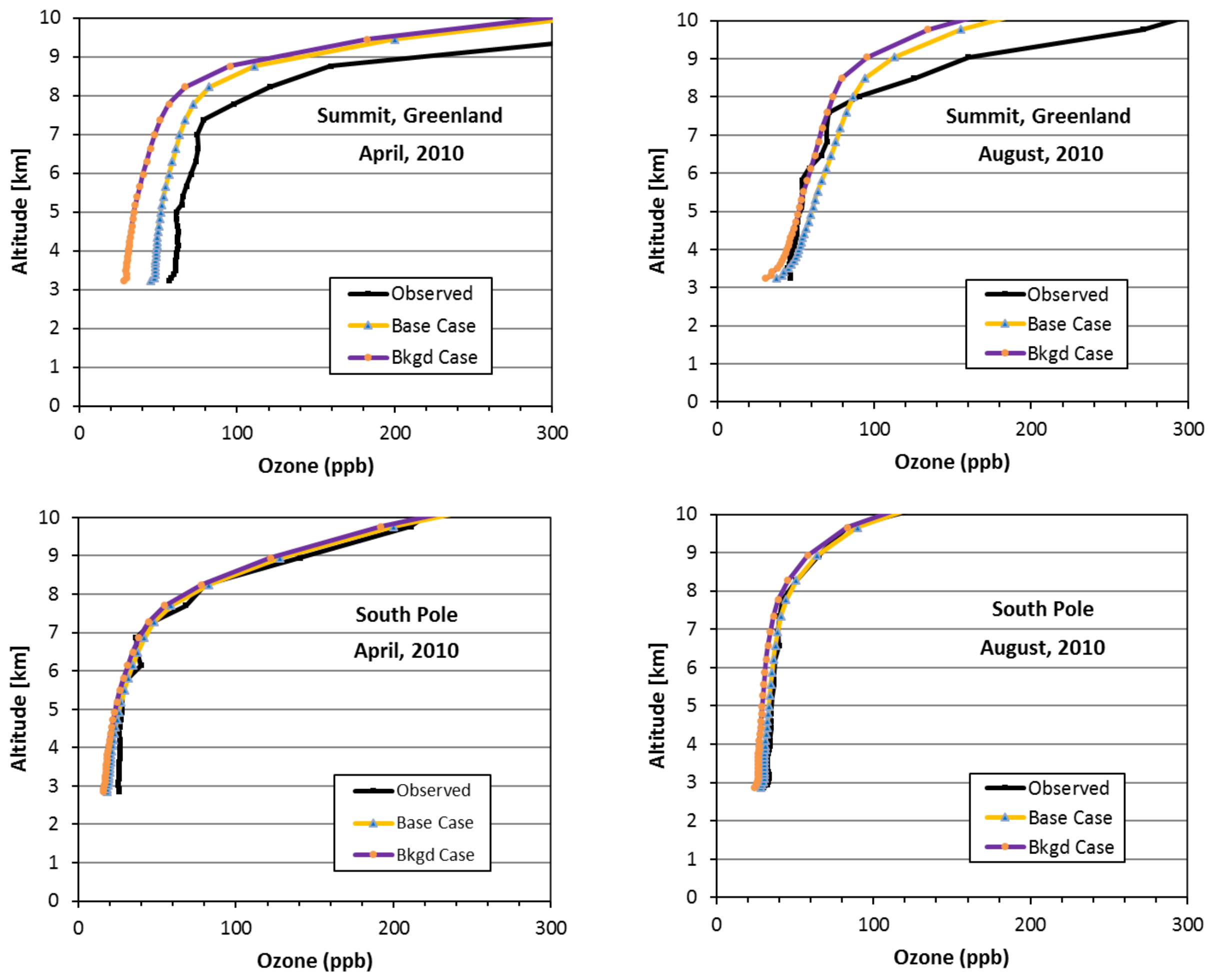

Figure S2. Comparison of GEOS-Chem vertical O_3 profiles for the base and background cases in April and August to ozonesonde measurements at two sites outside the CAMx domain. Monthly averages are shown. Locations and elevations of the sites are in Table S5.

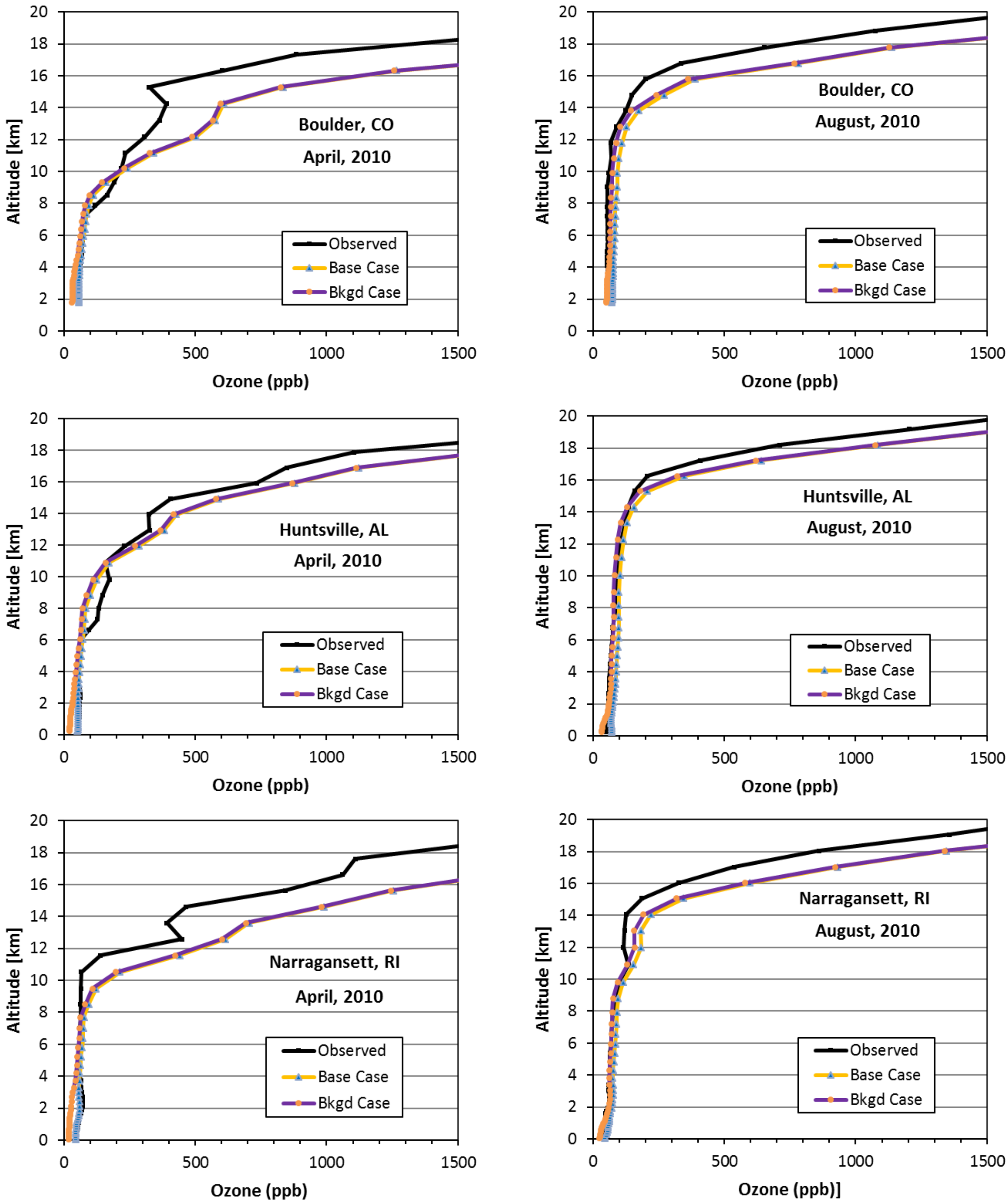

Figure S3. Comparison of GEOS-Chem vertical O_3 profiles for the base and background cases to ozonesonde measurements over an expanded altitude range. Monthly averages are shown.

Table S5. Locations and elevations of ozonesonde sites.

Site	Longitude	Latitude	Elevation above sea level (km)
Boulder, Colorado	-105.25	40.0	1.743
Hilo, Hawaii	-155.05	19.72	0.01
Huntsville, Alabama	-86.65	34.73	0.203
Narragansett, Rhode Island	-71.42	41.49	0.021
South Pole, Antarctica	169.	-90.	2.835
Summit, Greenland	-38.48	72.57	3.211
Trinidad Head, California	-124.16	40.8	0.02

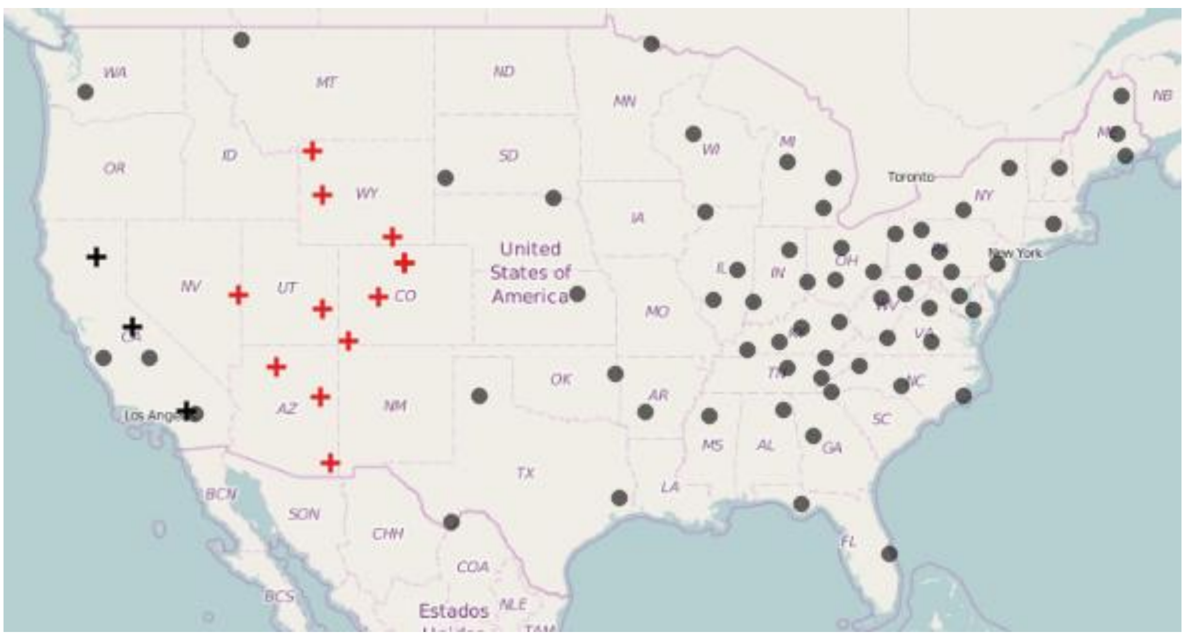

Figure S4. CASTNet monitoring sites. Sites with altitude below 1.5 km are circles and above 1.5 km are crosses. Red crosses indicate Intermountain West sites.

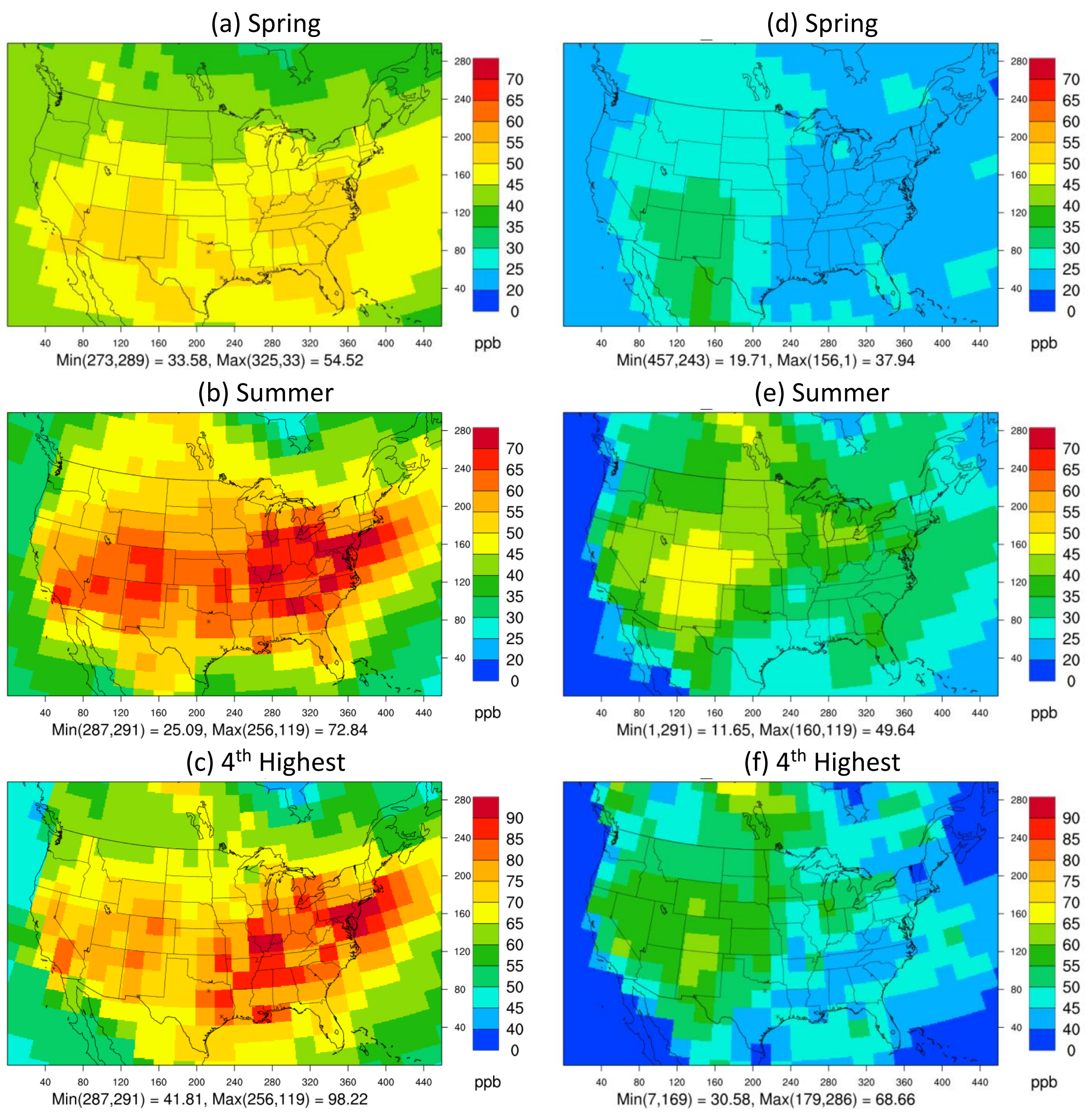

Figure S5. Spring (March–May) and summer (June–August) averages of MDA8 O_3 concentrations and 4th highest MDA8 O_3 from the G-Base (a–c) and G-Bkgd (d–f) GEOS-Chem simulations for 2010. Large O_3 concentrations over western Canada in summer are likely due to wildfires in northern Saskatchewan in July and early August.

Section S3. CAMx simulations

Table S6. Model performance for the CAMx base simulation at CASTNet and AQS sites in year 2010. Results are for MDA8 O_3 calculated with a 40-ppb threshold.

Season[a]	Network	N[b]	Mean Prediction (ppb)	NMB[c] (%)	NME[c] (%)	RMSE[c] (ppb)	R
			This work				
Spring	AQS	71,074.	49.8	-4.4	12.1	8.1	0.50
	CASTNet	5,737.	50.6	-4.9	12.3	8.3	0.49
Summer	AQS	72,548.	55.4	2.2	14.2	10.0	0.46
	CASTNet	5,029.	55.4	4.3	13.8	9.5	0.46
			Nopmongcol et al. (2017)[d]				
Spring	AQS	71,074.	53.6	2.7	10.9	7.4	0.61
	CASTNet	5,737.	54.2	1.9	10.3	7.1	0.63
Summer	AQS	72,548.	57.3	5.6	13.4	9.5	0.61
	CASTNet	5,029.	56.0	5.5	12.4	8.5	0.63

[a] Spring = March – May; summer = June – August

[b] Number of observations

[c] Normalized mean bias (NMB); normalized mean error (NME); root mean square error (RMSE)

[d] Nopmongcol, U., Liu, Z., Stoeckenius, T., and Yarwood, G.: Modeling inter-continental transport of ozone in North America with CAMx for the Air Quality Model Evaluation International Initiative (AQMEII) Phase 3, Atmos. Chem. Phys. Discuss., doi:10.5194/acp-2017-194, 2017.

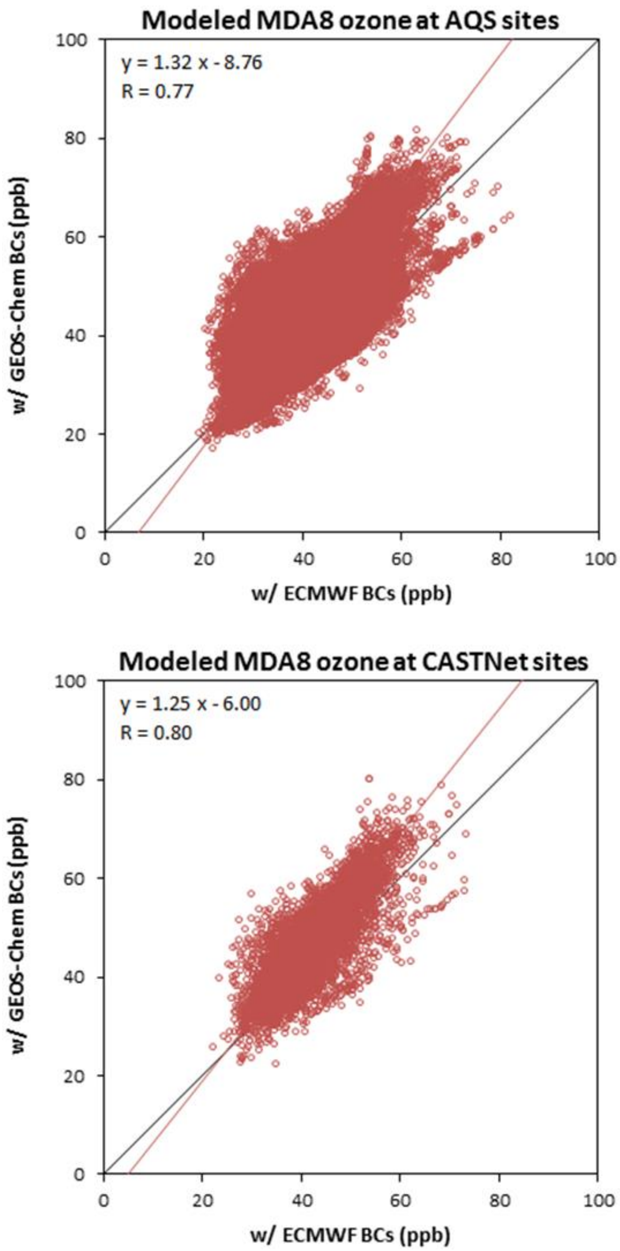

Figure S6. Scatter plots of modeled MDA8 O_3 concentrations using BCs from GEOS-Chem (this study) vs. BCs from the European Centre for Medium-Range Weather Forecasts (ECMWF) (Nopmongcol et al., 2017) for June–August 2010. In the CAMx simulations, deposition was included but chemistry and emissions were inactive. The red line is an orthogonal regression, which weights deviations in the x and y variables equally.

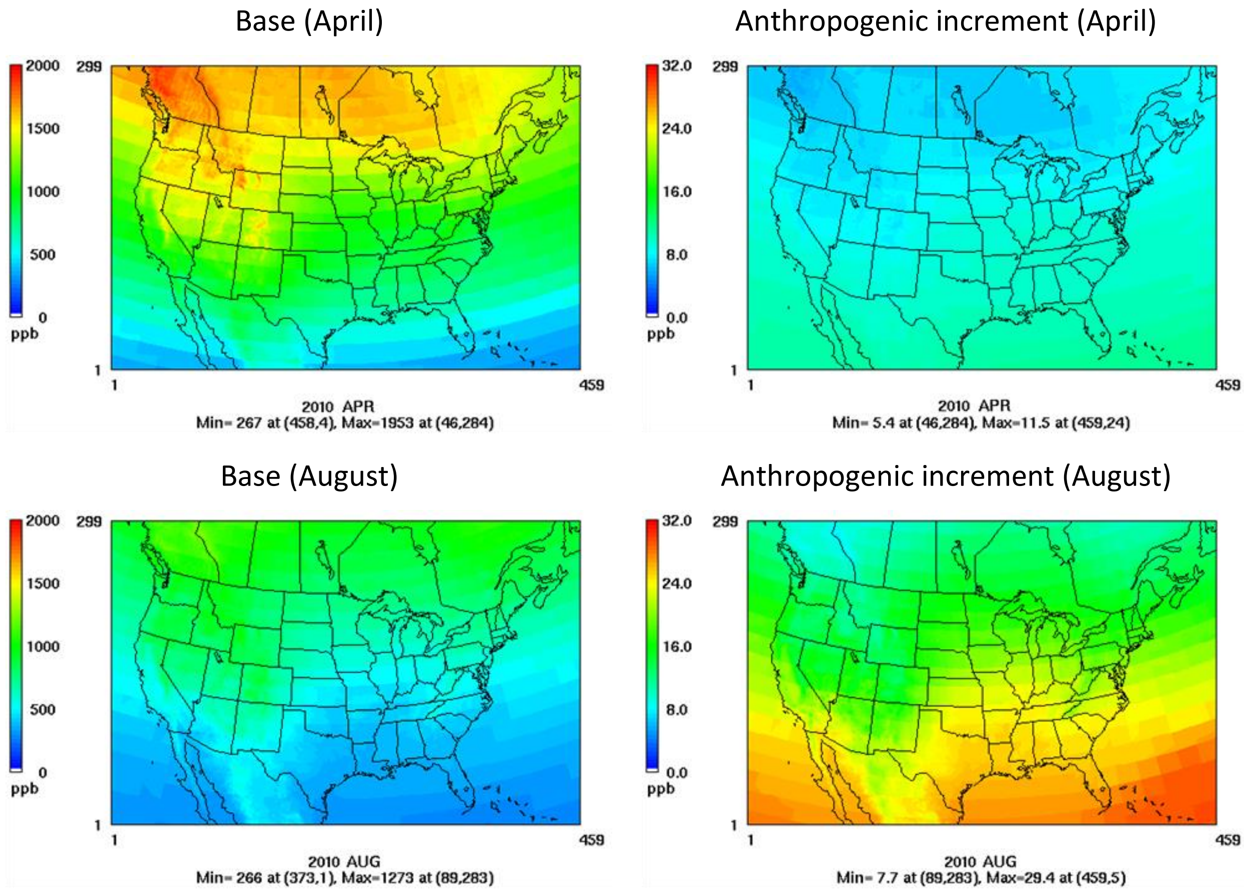

Figure S7. Monthly average O_3 concentrations for the top boundary of the CAMx domain from GEOS-Chem. Results are shown for the base case and the anthropogenic increment (difference between the base and background cases) in April and August.

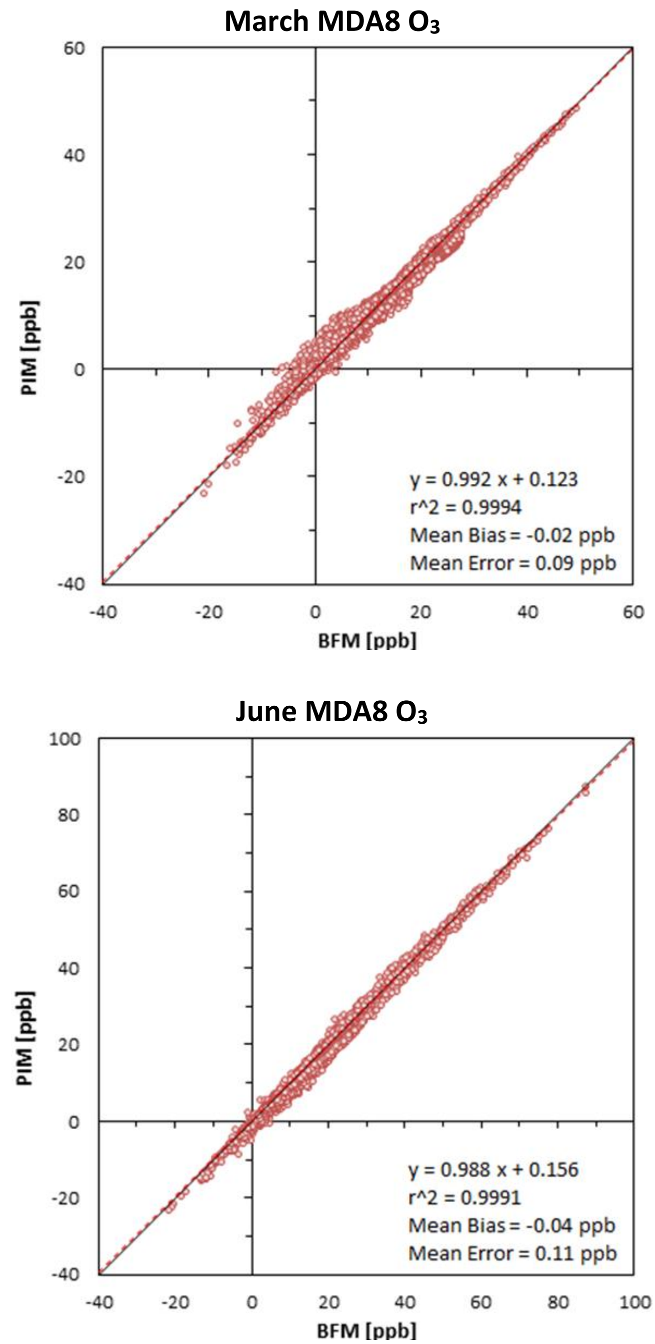

Figure S8. Comparison of the sum of the PIM source contributions for MDA8 O_3 in March and June, 2010, to the anthropogenic increment (brute-force method, BFM). Results are for all grid squares in the CAMx surface layer, and the red dashed line is the linear regression.

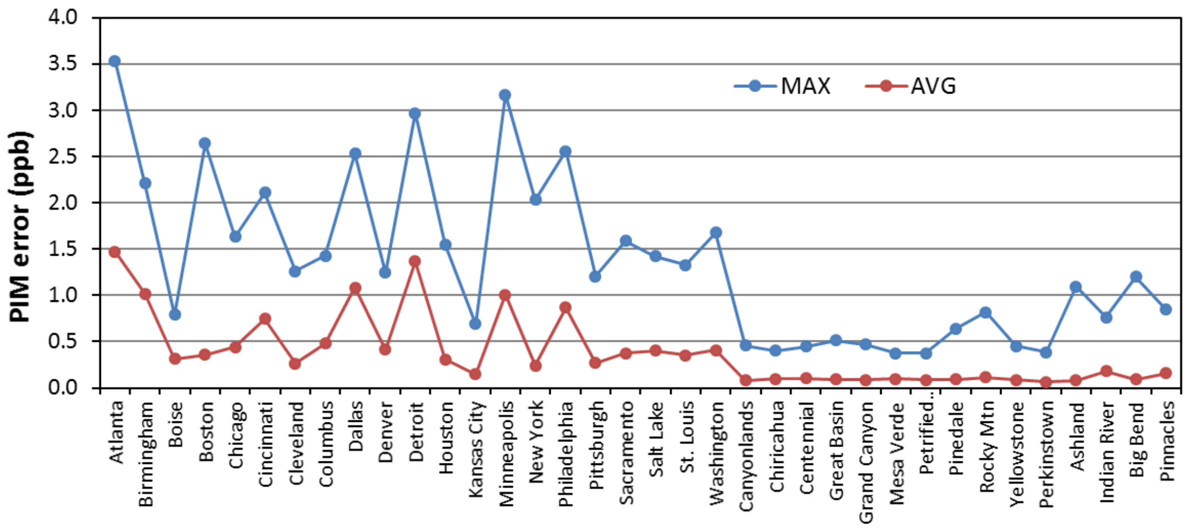

Figure S9. Maximum and average PIM error for March–September 2010 at the AQS and CASTNet sites. The error is the difference between the sum of the PIM source contributions for MDA8 O_3 and the anthropogenic increment.

Table S7. Site identification codes (IDs) for CASTNet and AQS sites in Table 3 and Figs. 10, S9, S14, and S15.

Site	Site ID	Latitude	Longitude
	AQS sites		
Atlanta, GA	131210055	33.72057	-84.3574
Birmingham, AL	10732006	33.38639	-86.8167
Boise, ID	160010017	43.5776	-116.178
Boston, MA	440090007	41.49167	-71.4278
Chicago, IL	550590019	42.50472	-87.8093
Cincinnati, OH	390610006	39.2785	-84.366
Cleveland, OH	390071001	41.95944	-80.5725
Columbus, OH	390490029	40.08667	-82.8156
Dallas, TX	484392003	32.9225	-97.2819
Denver, CO	80350004	39.53449	-105.07
Detroit, MI	261630019	42.43084	-83.0001
Houston, TX	480391004	29.52043	-95.3925
Kansas City, KS	290490001	39.5306	-94.556
Minneapolis, MN	270031002	45.13768	-93.2076
New York, NY	340290006	40.06485	-74.4441
Philadelphia, PA	421010024	40.07639	-75.0119
Pittsburgh, PA	420031005	40.61722	-79.7322
Sacramento, CA	60670012	38.68389	-121.163
Salt Lake, UT	490110004	40.90297	-111.884
St. Louis, MO	291831002	38.87255	-90.2265
Washington, DC	240251001	39.41	-76.2967
	CASTNet sites		
Ashland, ME	ASH135	46.6041	-68.4135
Big Bend NP, TX	BBE401	29.3022	-103.177
Canyonlands NP, UT	CAN407	38.4586	-109.821
Centennial, WY	CNT169	41.3642	-106.24
Chiricahua NM, AZ	CHA467	32.0092	-109.389
Grand Canyon NP, AZ	GRC474	36.0597	-112.182
Great Basin NP, NV	GRB411	39.0053	-114.216
Indian River Lagoon, FL	IRL141	27.8492	-80.4554
Mesa Verde NP, CO	MEV405	37.1983	-108.49
Perkinstown, WI	PRK134	45.2066	-90.5969
Petrified Forest, AZ	PET427	34.8225	-109.892
Pinedale, WY	PND165	42.9288	-109.788
Pinnacles NM, CA	PIN414	36.485	-121.156
Rocky Mtn NP, CO	ROM406	40.2778	-105.545
Yellowstone NP, WY	YEL408	44.5597	-110.401

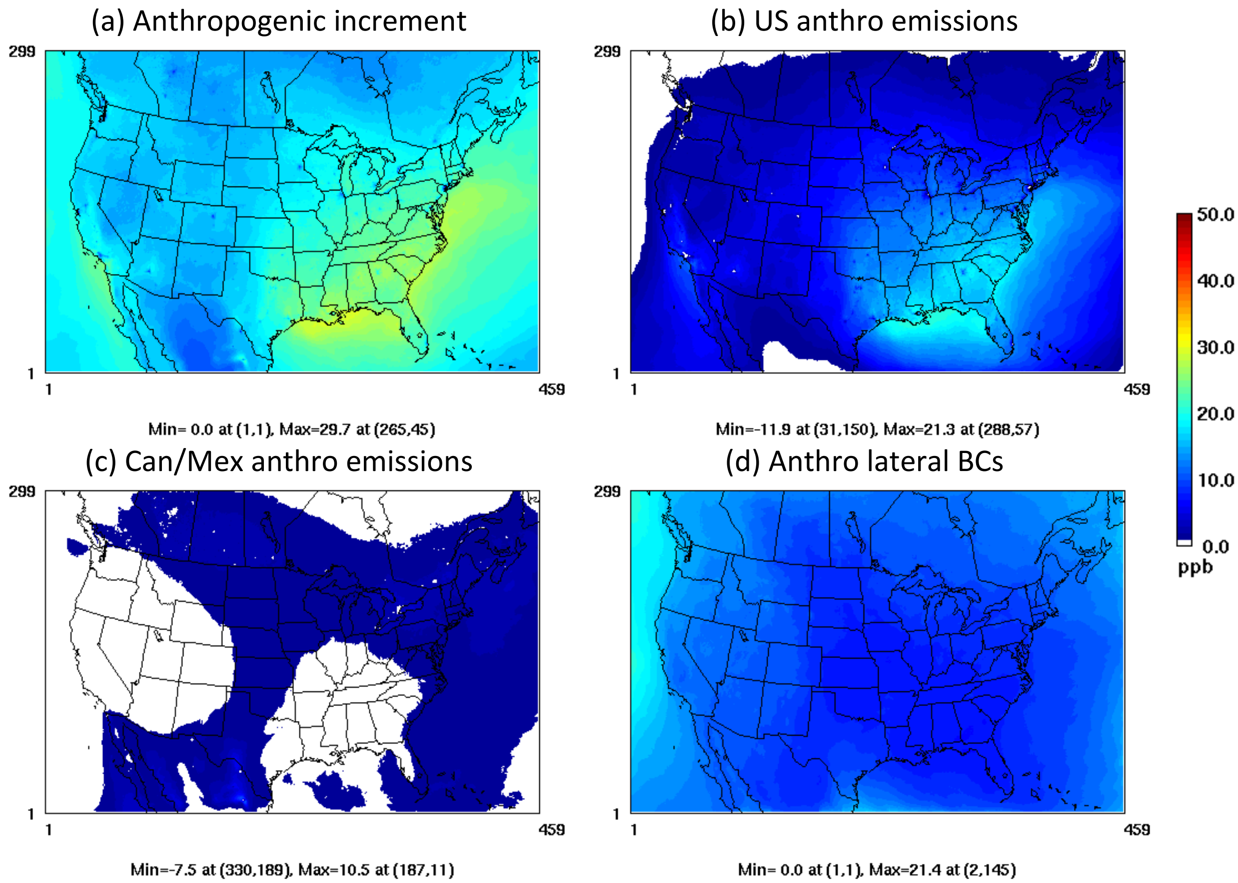

Figure S10. The anthropogenic increment (a) of the spring (March–May) MDA8 O_3 concentration and the contributions (b–d) to this increment. The contribution from the anthropogenic component of the top BCs (not shown) is ≤ 0.1 ppb.

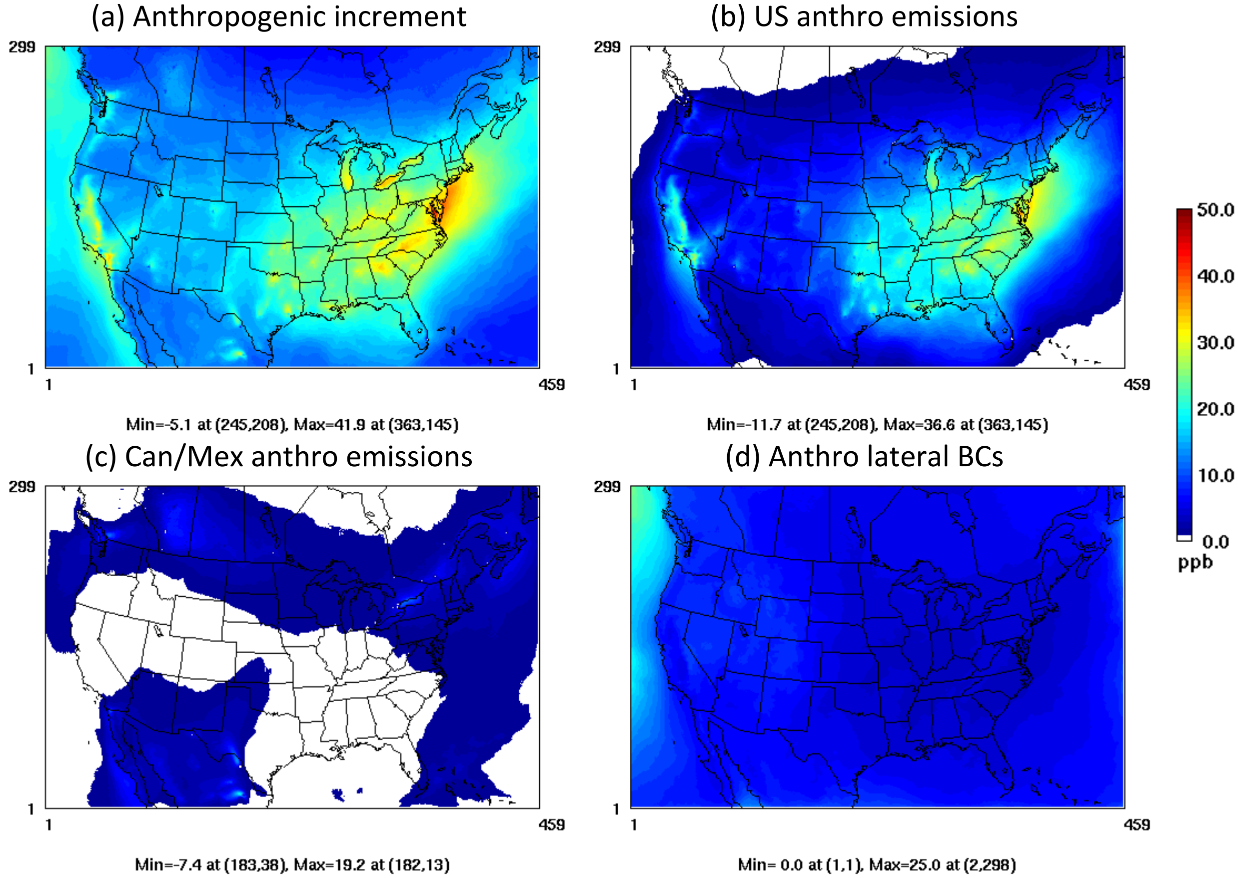

Figure S11. The anthropogenic increment (a) of the summer (June–August) MDA8 O_3 concentration and the contributions (b–d) to this increment. The contribution from the anthropogenic component of the top BCs (not shown) is ≤ 0.1 ppb.

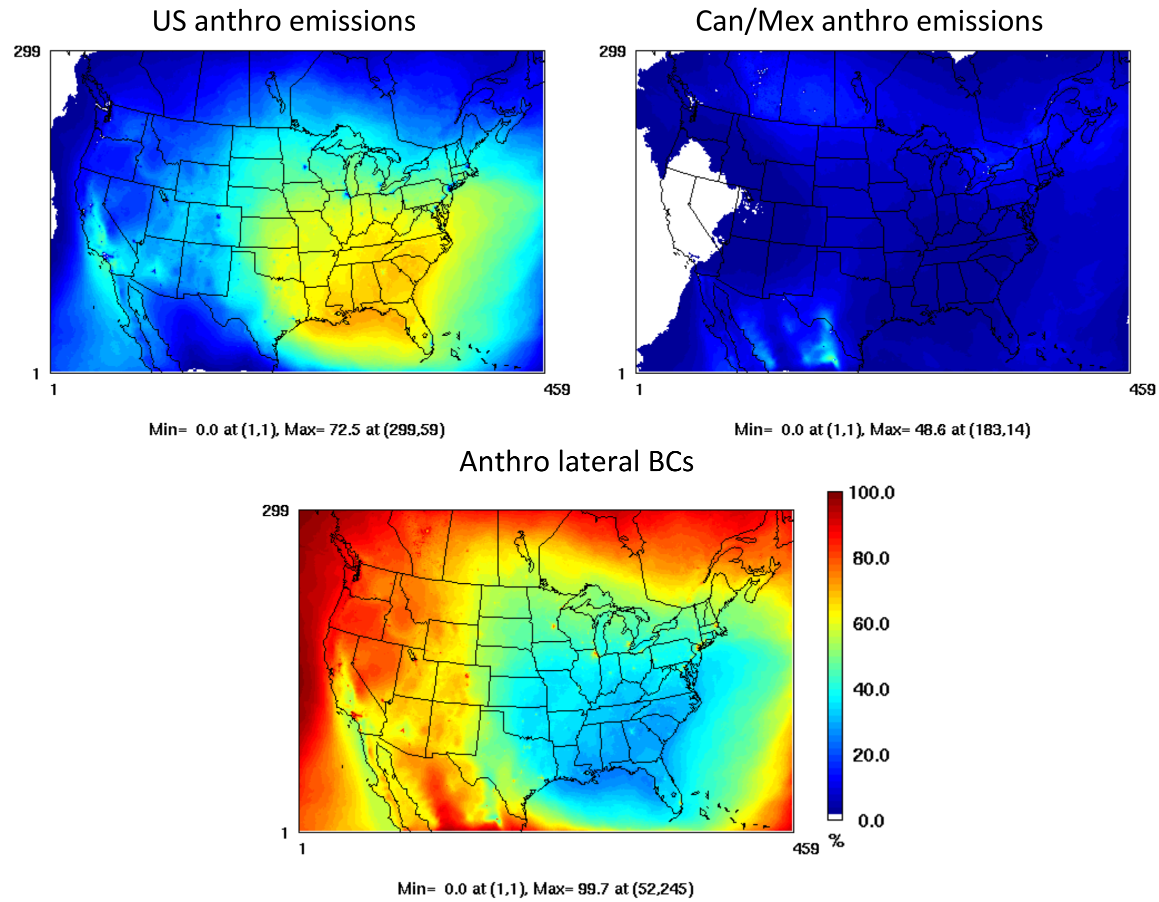

Figure S12. Relative contributions in percent to the anthropogenic increment of the spring MDA8 O_3 concentration. The contribution from the anthropogenic component of the top BCs (not shown) is ≤ 0.5%.

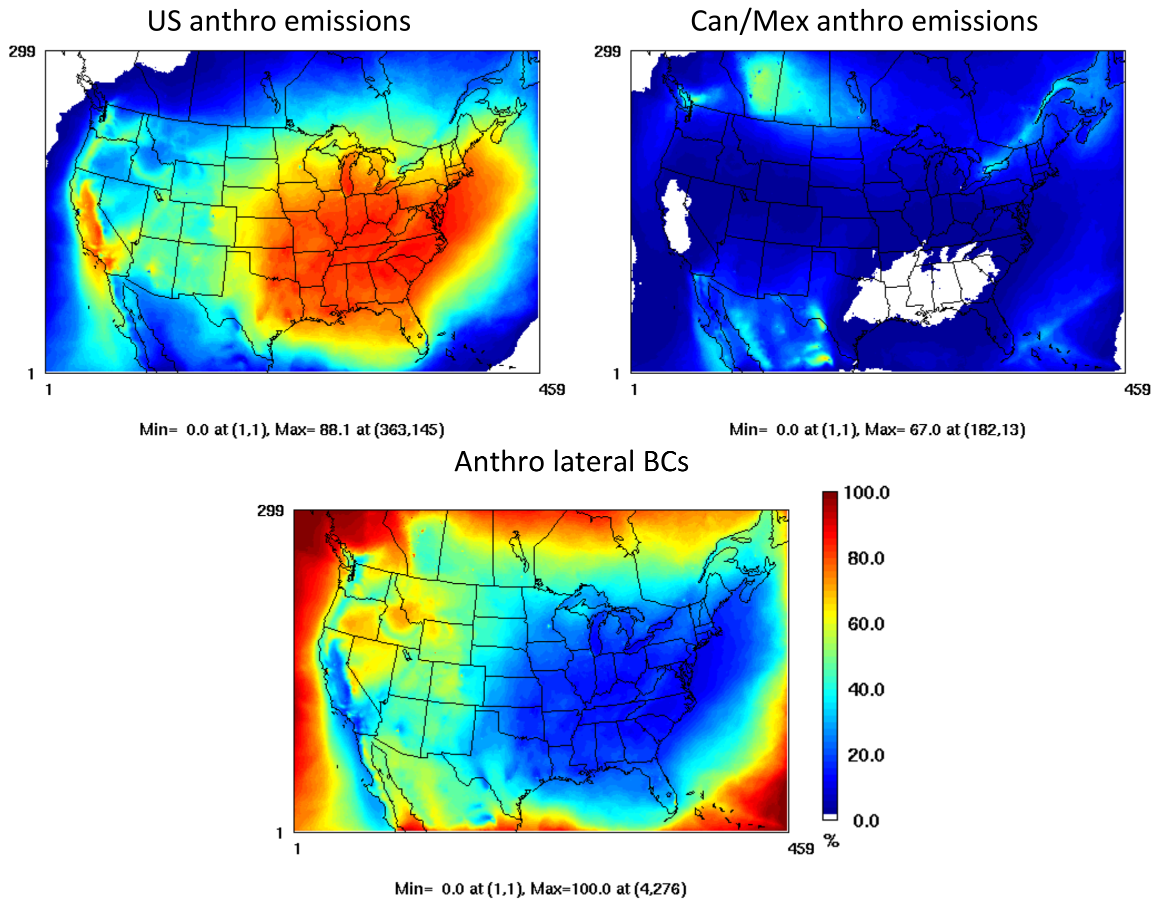

Figure S13. Relative contributions in percent to the anthropogenic increment of the summer MDA8 O_3 concentration. The contribution from the anthropogenic component of the top BCs (not shown) is ≤ 1%.

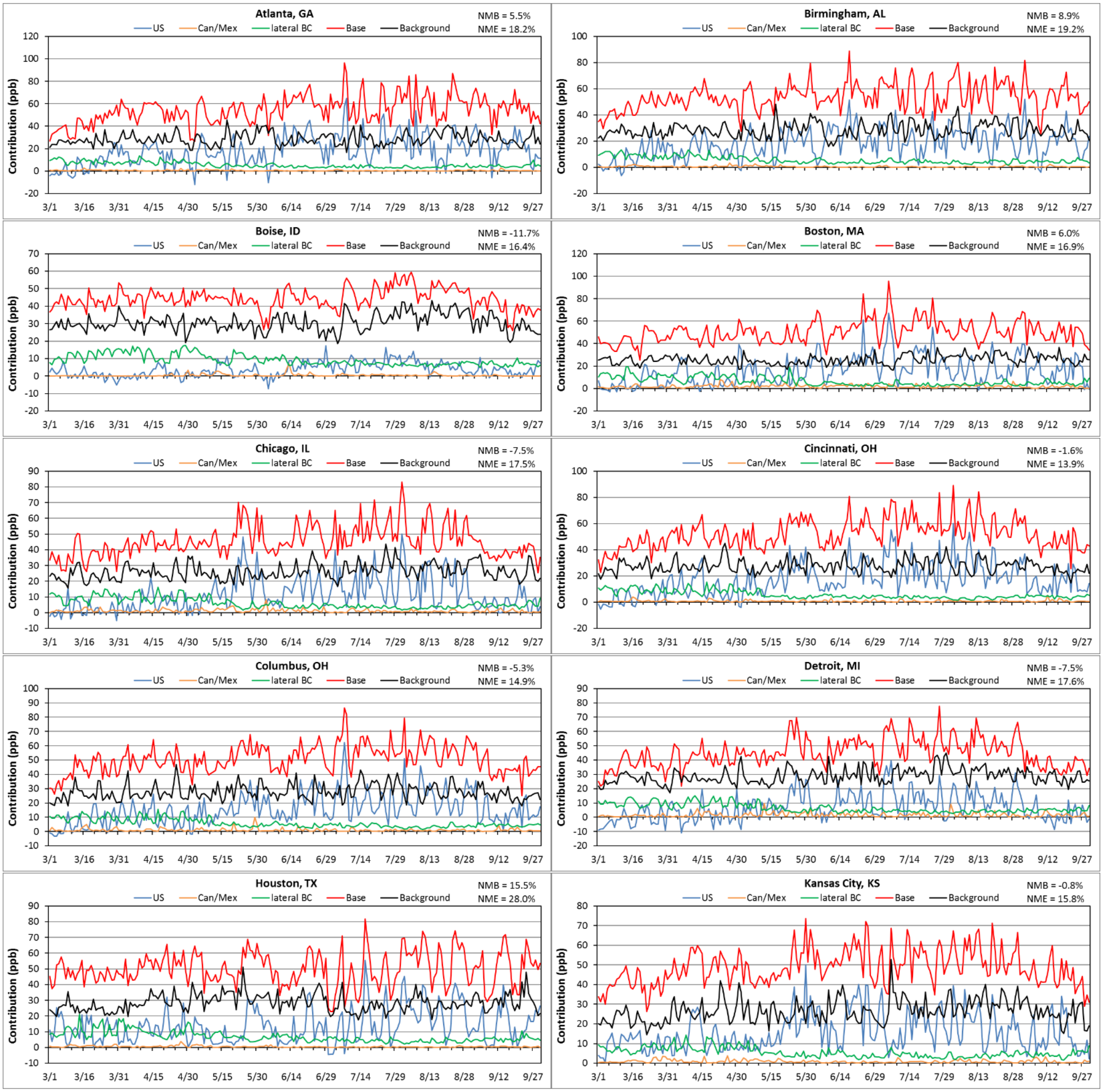

Figure S14. Anthropogenic contributions to MDA8 O_3 at AQS sites along with base-case and background concentrations.

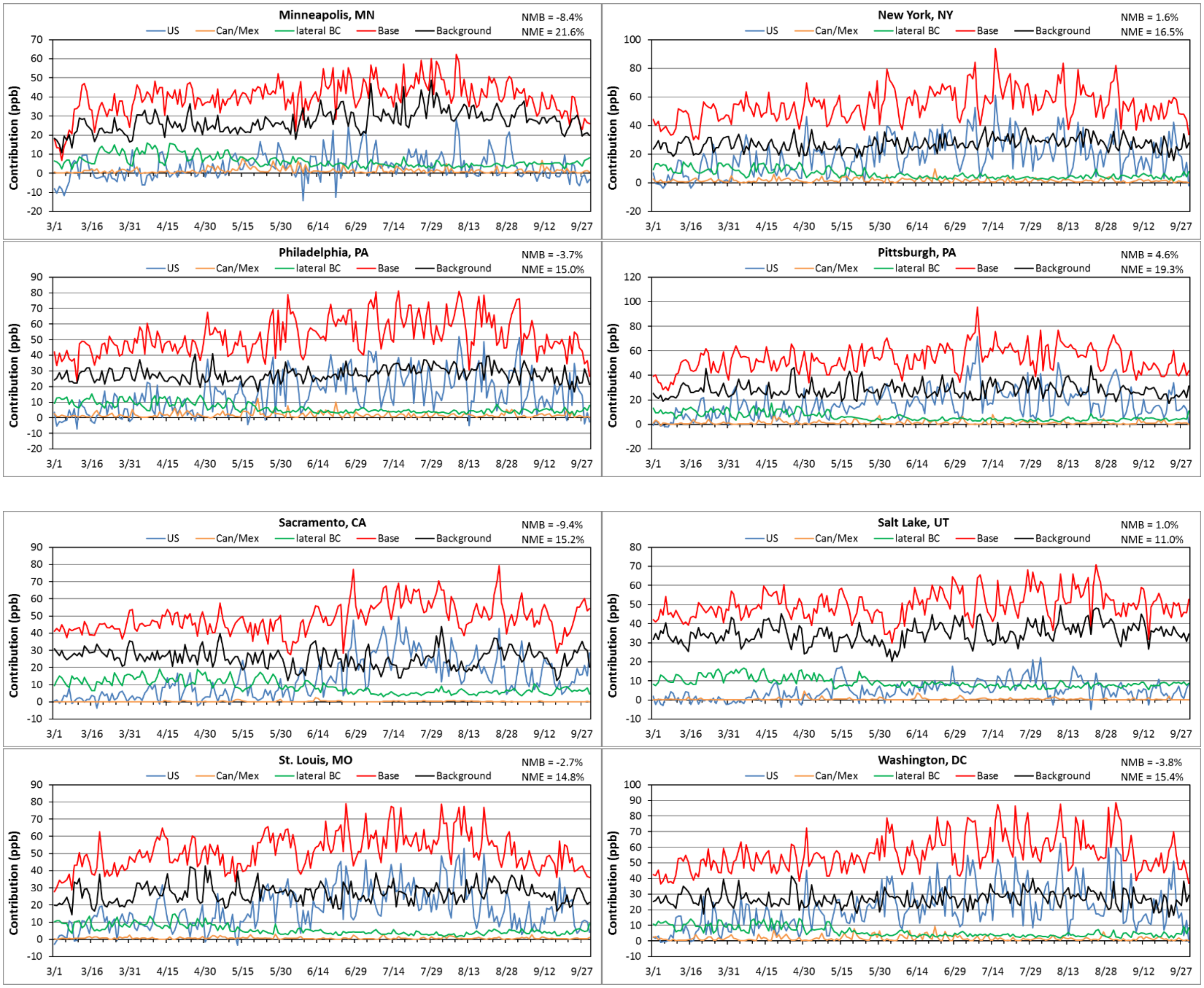

Figure S14 (concluded).

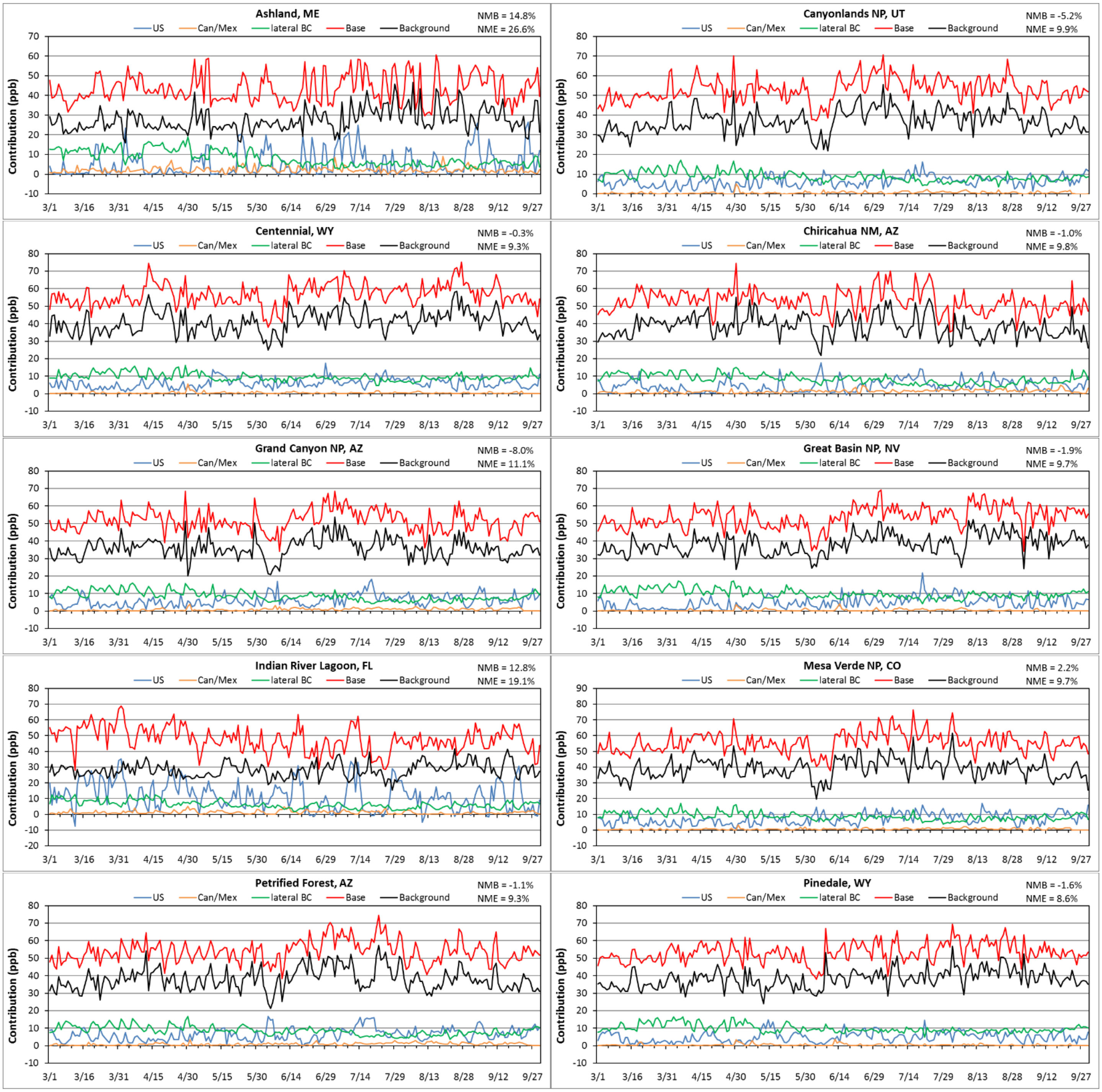

Figure S15. Anthropogenic contributions to MDA8 O_3 at CASTNet sites along with base-case and background concentrations.

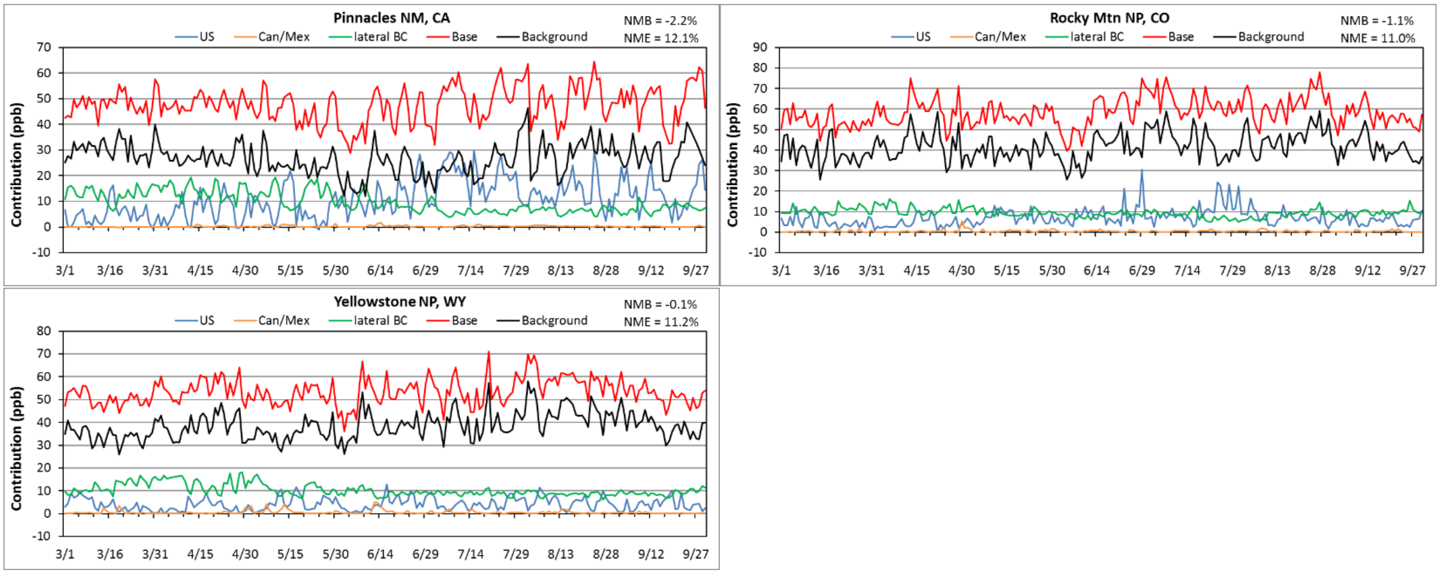

Figure S15 (concluded).